SUPPORTING MATERIAL FOR:
Furrow constriction in animal cell cytokinesis

Hervé Turlier,[†*] Basile Audoly,[‡] Jacques Prost,[†§] and Jean-François Joanny[†]

[†]Physicochimie Curie (CNRS-UMR168),
Institut Curie, Section de Recherche,
26 rue d'Ulm, 75248 Paris Cedex 05, France,

[‡]Institut Jean Le Rond d'Alembert (CNRS-UMR7190),
UPMC Université Paris 06,
4 Place Jussieu 75252 Paris Cedex 05, France,

[§]ESPCI-ParisTech,
10 Rue Vauquelin, 75231 Paris Cedex 05, France

[*]Correspondence: herve.turlier@polytechnique.org

This document contains:

- A Model Supplement and Supporting References
- Tables S1 and S2
- Figures S1 to S6
- Still images and legends for Movies S1 to S5

MODEL SUPPLEMENT

1 Continuous model

1.1 Model hypothesis

Negligible cytoplasmic dissipation Flows of the cytoplasm in cytokinesis are triggered by compression in the furrow region and by advection by cortical flows in polar regions. No matter which one of these processes is dominant, cytoplasmic flows are therefore passively driven by an active cortical flow of typical value v_a. The order of magnitude of the strain rate of cytoplasmic flows is therefore $\frac{v_\mathrm{a}}{R}$, where R is the mean curvature radius of the polar regions. Note that this scaling law also gives the strain rate of cortical flows from the poles toward the equator. Cytoplasmic flows operate on volumes of the order of cell volume R^3, whereas the typical cortical volume is $R^2 e_0$, where e_0 is the cortical thickness. We evaluate therefore the two sources of dissipation as follows

$$\mathcal{D}_\mathrm{cytoplasm} \approx \eta_\mathrm{cytoplasm} R^3 \left(\frac{v_\mathrm{a}}{R}\right)^2 , \tag{S1a}$$

$$\mathcal{D}_\mathrm{cortex} \approx \eta_\mathrm{actomyosin} R^2 e_0 \left(\frac{v_\mathrm{a}}{R}\right)^2 . \tag{S1b}$$

The ratio of the two sources of viscous dissipation, cytoplasmic and actomyosin cortical flows, scales finally as

$$\frac{\mathcal{D}_\mathrm{cytoplasm}}{\mathcal{D}_\mathrm{cortex}} \approx \frac{\eta_\mathrm{cytoplasm}}{\eta_\mathrm{actomyosin}} \frac{R}{e_0} . \tag{S2}$$

which is identical to the formula derived by Yeung and Evans in a more detailed analysis (1). The viscosity of the cortex is of the order of 10^5-10^6 $Pa.s$ (Table S1), whereas the cytoplasmic viscosity is of the order of 10^{-2}-10^1 $Pa.s$ (2–4). In spite of a high volume ratio $R/e_0 \approx 10^2$ (see Table S1), the viscous dissipation in the cytoplasm remains therefore generally negligible compared to the dissipation in the cortex during cytokinesis: $\mathcal{D}_\mathrm{cytoplasm} \ll \mathcal{D}_\mathrm{cortex}$.

We see from (Eq. S2) that for very big cells, the viscous dissipation in the cytoplasm might become important. We consider as an example an extreme case, a Xenopus Laevis egg, which might be the largest animal egg, with a diameter $R \sim 1\,mm$. Its cortex has a thickness e of the order of $\sim 100\,nm$ (23) and a viscosity at minimum $10^5\,Pa.s$. In normal conditions, the cytoplasm is expected to have a viscosity of the order of $10^1\,Pa.s$ at most. The ratio (Eq. S2) would then be of order ~ 1, indicating that viscous dissipation in the cytoplasm should start to be taken into account. Most of the cell lines studied have generally a diameter smaller than $100\,\mu m$ and the assumption of negligible cytoplasmic dissipation is not very restrictive.

Negligible friction on the plasma membrane A further possible source of dissipation is the friction of the cortex on the plasma membrane. In C. Elegans embryos, Mayer et al. (6) evaluated experimentally the hydrodynamic length scale of cortical flows $l \equiv \sqrt{\eta^{2\mathrm{D}}/\gamma}$, where $\eta^{2\mathrm{D}} \sim e_0 \eta_{actomyosin}$ is the 2D effective viscosity of the cortical layer and γ characterizes the frictional forces associated with cortical sliding along the cell membrane and the cytoplasm. The hydrodynamic length scale evaluates the typical length over which viscous dissipation dominates over frictional losses. Their measurements led to $l \approx 14\mu m$, which is about the embryo size: it indicates that friction forces are not limiting the cortical flow and hence can be neglected compared to cortical viscous forces. More generally the extension of cortical flows over the entire cell during cytokinesis, as early reported in sea-urchin eggs (7–9), reveals negligible friction losses compared to cortical viscous dissipation.

1.2 Lagrangian formulation of an axisymmetric visco-active membrane shell

We follow the geometric approach developed originally in (10) to describe the dynamics of thin viscous threads, and we adapt it to axisymmetric thin shells. The mechanical equilibrium of viscous thin shells is

given by the balance of forces normal and tangential to the shell contour. Because the shell remains thin, stresses can be integrated over its thickness, which leads to tensions acting tangentially to the shell mid-surface (11). A membrane is a thin shell where the contribution of bending moments and transverse shear components are negligible compared to in-plane tensions (11). The cortical layer was already described by an Eulerian membrane theory by Yeung and Evans (1), and by a thin shell theory, explicitely derived by Salbreux (12) from the active-gel rheology (13), but with fixed thickness (no turnover) and at leading order in perturbation. We elaborate here continuous and discrete Lagrangian membrane formulations, allowing for shell thickness variations via explicit turnover, and we solve the problem numerically in the regime of large deformations and large displacements.

1.2.1 Lagrangian description

A Lagrangian description requires the definition of a reference state. It is chosen here to be spherical, corresponding to the metaphase cell shape, right before cytokinesis onset. Since the membrane remains axisymmetric, its shape in 3D can be reconstructed by revolving a base curve about the z-axis $\mathbf{e}_z$ (Fig. S1 *A* and Movie S5). We call φ the azimuthal angle. We consider therefore only a section plane $(\mathbf{e}_z, \mathbf{e}_r(\varphi))$ perpendicular to the azimuthal direction $\mathbf{e}_\varphi(\varphi)$ (Fig. S1 *A*).

We call S the Lagrangian curvilinear coordinate in the reference state of the membrane, to distinguish from the Eulerian curvilinear or contour length s used in the main text and defined in the next section.

Spatial and temporal derivatives of any function $f(S,t)$ are defined by

$$f'(S,t) = \frac{\partial f(S,t)}{\partial S}\,, \tag{S3a}$$

$$\dot{f}(S,t) = \frac{\partial f(S,t)}{\partial t}\,. \tag{S3b}$$

Since S is a Lagrangian variable, the time derivative is a *material* derivative - often writen $\dot{f}(S,t) = \frac{Df(s,t)}{Dt}$ in an Eulerian formulation - and describes the rate of change of f as one follows a particle.

1.2.2 Membrane kinematics

In actual configuration, the position of the membrane reads

$$\mathbf{x}(S,t) = z(S,t)\,\mathbf{e}_z + r(S,t)\,\mathbf{e}_r(\varphi)\,. \tag{S4}$$

Its first and second time derivatives are the *material* velocity and acceleration:

$$\mathbf{u}(S,t) = \dot{\mathbf{x}}(S,t) = (\dot{z}(S,t), \dot{r}(S,t))\ , \tag{S5a}$$

$$\ddot{\mathbf{x}}(S,t) = \dot{\mathbf{u}}(S,t) = (\ddot{z}(S,t), \ddot{r}(S,t))\ . \tag{S5b}$$

We define the local Frenet frame $(\mathbf{t}, \mathbf{n}, \mathbf{e}_\varphi)$, where $\mathbf{t}$ and $\mathbf{n}$ are the unit vectors tangent and normal to the midline (Fig. S1 *A*).

$$\mathbf{t}(S,t) = \frac{\mathbf{x}'}{|\mathbf{x}'|} = \frac{\mathbf{x}'(S,t)}{\ell(S,t)}\,, \tag{S6a}$$

$$\mathbf{n}(S,t) = \mathbf{e}_\varphi \times \mathbf{t}(S,t)\,. \tag{S6b}$$

where $\ell(S,t) = |\mathbf{x}'(S,t)|$ measures the stretch of the base curve, compared to the reference configuration.

We define the curvilinear or contour length s (Main text Eq. 2 and *(inset)* of Figs. 3 *A*, 4 and 5) using the equator as the origin: $s(S,t) = \int_{S_{\rm eq}}^{S} dS'\,\ell(S',t)$, where $S_{\rm eq}$ denotes the Lagrangian coordinate of the equator.

The area of the membrane per unit dS and $d\varphi$ is given by

$$a = \left|\mathbf{x}' \times \mathbf{x}_{,\varphi}\right| = |\ell\,\mathbf{t} \times (-r\,\mathbf{e}_\varphi)| = \ell(S,t)\,r(S,t)\,. \tag{S7}$$

where $f_{,\varphi} \equiv \frac{\partial f}{\partial \varphi}$

The rate of membrane stretching reads therefore

$$\frac{\dot{a}}{a} = \frac{\dot{\ell}}{\ell} + \frac{\dot{r}}{r}\,, \tag{S8}$$

where $\dot{\ell} = \left|\frac{\partial^2 \mathbf{x}}{\partial S \partial t}\right| = \left|\frac{\partial \mathbf{u}}{\partial S}\right| = \mathbf{t} \cdot \frac{\partial \mathbf{u}}{\partial S}$.

By identification we deduce the two components $d_s + d_\varphi = \frac{\dot{a}}{a}$ of the membrane strain rate in axial direction $\mathbf{t}$ and azimuthal direction $\mathbf{e}_\varphi$

$$d_s(S,t) = \frac{\dot{\ell}}{\ell} = \mathbf{t} \cdot \left(\frac{1}{\ell}\frac{\partial \mathbf{u}}{\partial S}\right)\,, \tag{S9a}$$

$$d_\varphi(S,t) = \frac{\dot{r}}{r} = \mathbf{e}_r \cdot \frac{\mathbf{u}}{r}\,. \tag{S9b}$$

1.2.3 Membrane tensions

The tension in the membrane is obtained by integrating the bulk actomyosin stress $\sigma_{\alpha\beta}$ in its transverse dimension ξ along $\mathbf{n}$. Given that the cortex remains thin relative to the cell radius, we only keep the first order in thickness $e(S,t)$ in a membrane theory. Axial and azimuthal tension components read, respectively,

$$N_s(S,t) = \int_{-e/2}^{e/2} d\xi\, \sigma_{ss}(\xi) \approx e\sigma_{ss}(0)\,, \qquad N_\varphi(S,t) = \int_{-e/2}^{e/2} d\xi\, \sigma_{\varphi\varphi}(\xi) \approx e\sigma_{\varphi\varphi}(0)\,. \tag{S10}$$

where the mid-surface is defined at $\xi = 0$. The stress in an actomyosin gel is the sum of viscous and active components, as explained below.

2D reduction of the viscous constitutive law We write the constitutive relation for a Stokean fluid in 3 dimensions (14)

$$\sigma^v_{\alpha\beta} = 2\eta\, u^v_{\alpha\beta} - p\,\delta_{\alpha\beta}\,, \tag{S11}$$

where $\sigma^v_{\alpha\beta}$ is the viscous contribution to the bulk viscous stress in the gel, p the bulk pressure and $u^v_{\alpha\beta} \equiv \frac{1}{2}\left(\partial_\alpha u_\beta + \partial_\beta u_\alpha\right)$ the symmetric part of the bulk strain rate tensor in the gel.

In the Frenet frame $(\mathbf{t}, \mathbf{n}, \mathbf{e}_\varphi)$, the incompressibility of the gel reads

$$u^v_{ss} + u^v_{\varphi\varphi} + u^v_{nn} = 0\,. \tag{S12}$$

The normal component of the stress vanishes at the free boundaries $\sigma_{nn}(e/2) = \sigma_{nn}(-e/2) = 0$ and is considered uniform along the transverse direction in a membrane theory (lubrication hypothesis). We deduce the bulk pressure

$$p \approx 2\eta\, u^v_{nn} = -2\eta\left(u^v_{ss} + u^v_{\varphi\varphi}\right). \tag{S13}$$

The membrane's strain rates in the axial and azimuthal directions are defined by averaging the bulk strain rate over the thickness, and can be identified with strain rates at the mid-surface at the dominant order, $d_s = \frac{1}{e}\int_{-e/2}^{e/2} d\xi\, u_{ss}(\xi) \approx u^v_{ss}(0)$ and $d_\varphi = \frac{1}{e}\int_{-e/2}^{e/2} d\xi\, u_{\varphi\varphi}(\xi) \approx u^v_{\varphi\varphi}(0)$. This yields the effective 2D viscosity law for the membrane,

$$N^v_s = 2\,\eta\, e\,(2\,d_s + d_\varphi)\,, \tag{S14a}$$

$$N^v_\varphi = 2\,\eta\, e\,(d_s + 2\,d_\varphi)\,. \tag{S14b}$$

Active constitutive law A nematic theory of active gels (13) predicts an active stress dominant contribution of the general form

$$\sigma^a_{\alpha\beta} = \zeta \Delta\mu \, Q_{\alpha\beta} \,, \tag{S15}$$

where $Q_{\alpha\beta} \equiv \left\langle p_\alpha p_\beta - \frac{1}{3}\delta_{\alpha\beta} \right\rangle$ is the nematic order parameter, $\zeta > 0$ is a measure of the local motor contractile activity, $\Delta\mu$ is the chemical free energy for one ATP molecule hydrolysis and p_α is a vector representing the local polarity of filaments. We make the simplifying assumption that actin filaments remain parallel to the membrane mid-plane and that their polarization remains isotropic within the membrane plane. This implies $Q_{ss} = Q_{\varphi\varphi} = \frac{1}{2}$ and $Q_{nn} = 0$.

The active contribution to the membrane tension is therefore isotropic and reads

$$N^a_s = N^a_\varphi \approx e \, \sigma^a_{ss}(0) = e \, \sigma^a_{\varphi\varphi}(0) = \frac{e}{2} \zeta(S,t) \Delta\mu \,. \tag{S16}$$

Membrane total tension The total tensions in the membrane are the sum of the active (Eq. S16) and viscous (Eq. S14) contributions and read (Main text Eq. 2)

$$N_s = \frac{e}{2} \zeta \Delta\mu + 2\,\eta\, e\,(2\,d_s + d_\varphi) \,, \tag{S17a}$$

$$N_\varphi = \frac{e}{2} \zeta \Delta\mu + 2\,\eta\, e\,(d_s + 2\,d_\varphi) \,. \tag{S17b}$$

1.2.4 Turnover dynamics

The cortical actomyosin is under permanent turnover. The source term, due to actin polymerization, is proportional to the membrane surface since polymerization nucleators are located near the plasma membrane. We describe this effect via a polymerization velocity v_p from the shell upper surface $\xi = e/2$. By contrast depolymerization acts in volume and leads to a depolymerization rate k_d. The transverse strain rate in the membrane is therefore the sum of a viscous contribution and turnover term, whereas other strain rate components remain identical

$$u_{nn} = u^v_{nn} + \left[v_\mathrm{p}\, \delta\left(\xi - \frac{e}{2}\right) - k_\mathrm{d} \right] \,, \tag{S18}$$

where $\delta(x)$ is a Delta function of x.

We average over the membrane thickness the equation of incompressibility projected on the local Frenet frame $(\mathbf{t}, \mathbf{n}, \mathbf{e}_\varphi)$, which leads to

$$u_{ss}(0) + u_{nn}(0) + u_{\varphi\varphi}(0) = \frac{v_\mathrm{p}}{e} - k_\mathrm{d} \,. \tag{S19}$$

We consider a element of membrane of volume $a\,e = \ell(S,t)\, r(S,t)\, e(S,t)$ per unit dS and $d\varphi$, where the element of surface a is defined in Eq. S7. We identify the rate of surface stretching $d_s + d_\varphi = u^v_{ss}(0) + u^v_{\varphi\varphi}(0) = u_{ss}(0) + u_{\varphi\varphi}(0) = \frac{\dot{a}}{a}$ and the rate of thickness variation $u_{nn}(0) = \frac{\dot{e}}{e}$. We deduce the Lagrangian rate of variation of the element of membrane volume ae under both effects of incompressibility and turnover (Main text Eq. 3)

$$\frac{d\,(a\,e)}{dt} = -k_\mathrm{d}\, ae + v_\mathrm{p}\, a \,. \tag{S20}$$

1.3 Balance of forces

We use the principle of virtual work for thin membranes, as it provides a natural way to obtain the equations of motion for discrete membranes. For any virtual motion of the membrane $\hat{\mathbf{u}}(S,t) = \hat{\dot{\mathbf{x}}}$ subject to the constraint of incompressibility, the balance of forces in weak form reads (Einstein notation) (15)

$$-\oint dA\, N_{\alpha\beta} \hat{d}_{\alpha\beta} - K\,(\mathcal{V} - \mathcal{V}_0)\, \hat{\dot{\mathcal{V}}} = 0 \,. \tag{S21}$$

where $\hat{d}_{\alpha\beta} = \hat{u}_{\alpha\beta} = \frac{1}{2}\left(\partial_\alpha \hat{u}_\beta + \partial_\beta \hat{u}_\alpha\right)$ is the virtual strain rate, $\hat{\dot{\mathcal{V}}} = \oint dA\, n_\beta \hat{u}_\beta$ is the virtual change of volume, and $\oint$ is the integral on the closed membrane surface.

The divergence operator $\mathbf{div}\,(N_s, N_\varphi)$ is defined by the identity

$$\oint dA\, \mathbf{div}\,(N_s, N_\varphi) \cdot \hat{\mathbf{u}} = -\oint dA\, \left(N_s \hat{d}_s + N_\varphi \hat{d}_\varphi\right)$$

which must hold for any virtual displacement $\hat{\mathbf{u}}$ associated with the virtual strain rates $\hat{d}_s$ and $\hat{d}_\varphi$. Inserting the explicit expressions of the virtual strain rates, we find

$$\begin{aligned}\int 2\pi r\ell\, dS\, \mathbf{div}\,(N_s, N_\varphi) \cdot \left(\hat{\dot{z}}\mathbf{e}_z + \hat{\dot{r}}\mathbf{e}_r\right) &= -\int 2\pi r\ell\, dS \left(N_s \frac{\mathbf{t}}{\ell} \cdot \frac{\partial \hat{\mathbf{u}}}{\partial S} + N_\varphi \frac{\hat{\dot{r}}}{r}\right) \\ &= \int 2\pi r\ell\, dS \left\{\hat{\dot{z}}\left[-\frac{1}{r\ell}\frac{\partial}{\partial S}\left(r t_z N_s\right)\right] + \hat{\dot{r}}\left[\frac{N_\varphi}{r} - \frac{1}{r\ell}\frac{\partial}{\partial S}\left(r t_r N_s\right)\right]\right\},\end{aligned}$$

Identifying both sides, we find an explicit expression of the divergence operator (Main text Eq. 5):

$$\mathbf{div}\,(N_s, N_\varphi) = -\frac{1}{r\ell}\frac{\partial}{\partial S}\left(r t_z N_s\right)\, \mathbf{e}_z + \left(\frac{N_\varphi}{r} - \frac{1}{r\ell}\frac{\partial}{\partial S}\left(r t_r N_s\right)\right) \cdot \mathbf{e}_r. \tag{S22}$$

The principle of virtual work (Eq. S21) yields the force balance for membranes. It classically reads as in (Main text Eq. 5), where the divergence operator is given here by Eq. S22 in our representation.

2 Discrete formulation

We extend here the discretization approach proposed for viscous threads (10) to the case of axisymmetric membranes, based on the previous continuous equations.

2.1 Geometrical relations

The axisymmetric membrane shell is represented by a collection of $n+1$ vertices $\{\mathbf{x}_i(t) = (r_i(t), z_i(t))\}_{0\le i\le n}$ living in the half-plane $r \ge 0$ as represented on Fig. S1 *B*. Neighboring vertices are connected by segments. The vertices at poles $\mathbf{x}_0$ and $\mathbf{x}_n$ are subjected to the constraint $r_0 = r_n = 0$.

The volume enclosed by the membrane reads

$$\mathcal{V} = \sum V^i = \sum V(\mathbf{x}_i, \mathbf{x}_{i+1})\,, \tag{S23}$$

where the contribution associated with a segment is the volume enclosed by a truncated cone obtained by revolving the segment about the z-axis,

$$V(\mathbf{x}_i, \mathbf{x}_{i+1}) = \frac{\pi}{3}\left({r_i}^2 + r_i\, r_{i+1} + {r_{i+1}}^2\right)\left(z_{i+1} - z_i\right). \tag{S24}$$

Let us call $\mathbf{g}_i$ the gradient of the enclosed volume with respect to vertex positions. It will be used to define a discrete pressure force:

$$\mathbf{g}_i = \nabla_{\mathbf{x}_i} \mathcal{V}\,. \tag{S25}$$

It can be computed by summing contributions of the form

$$\mathbf{V}_{,i+1}(\mathbf{x}_i, \mathbf{x}_{i+1}) = \frac{\pi}{3}\left(\left(r_i + 2\, r_{i+1}\right)\left(z_{i+1} - z_i\right)\mathbf{e}_r + \left({r_i}^2 + r_i\, r_{i+1} + {r_{i+1}}^2\right)\mathbf{e}_z\right), \tag{S26}$$

and the symetric formula for $V_{,i}(\mathbf{x}_i, \mathbf{x}_{i+1})$. Here, the comma in index denotes a gradient with respect to a vertex $\mathbf{x}_i$: $\nabla_{\mathbf{x}_i} f = f_{,\mathbf{x}_i}$.

The area of the membrane reads

$$\mathcal{A} = \sum A^i = \sum A(\mathbf{x}_i, \mathbf{x}_{i+1})\,, \tag{S27}$$

where the contribution associated with a segment is the lateral area of a truncated cone,

$$A(\mathbf{x}_i, \mathbf{x}_{i+1}) = 2\,\pi\,\frac{r_i + r_{i+1}}{2}\,\ell^i\,, \tag{S28}$$

with

$$\ell^i = \sqrt{(r_{i+1} - r_i)^2 + (z_{i+1} - z_i)^2}\,, \tag{S29}$$

denotes the segment length.

2.2 Membrane strain rates

From the continuous formula in Eq. S9, we deduce the discrete strain rates in the axial and azimuthal directions

$$d_s^i = \frac{\dot{\ell}^i}{\ell^i} = \frac{\mathbf{t}^i \cdot (\mathbf{u}_{i+1} - \mathbf{u}_i)}{\ell^i}\,. \tag{S30a}$$

$$d_\varphi^i = \frac{\dot{r}_i + \dot{r}_{i+1}}{r_i + r_{i+1}} = \frac{\mathbf{e}_r \cdot (\mathbf{u}_i + \mathbf{u}_{i+1})}{r_i + r_{i+1}}\,. \tag{S30b}$$

2.3 Membrane tension

Viscous contribution From the continuous formulation in Eq. S14, the viscous contributions to the membrane tension read

$$N_s^{v\,j} = 2\,\eta\,e^j\,(2d_s^j + d_\varphi^j), \qquad N_{v\varphi}^j = 2\,\eta\,e^j\,(d_s^j + 2d_\varphi^j)\,. \tag{S31}$$

Active contribution From the continuous formulation in Eq. S16, the active contributions to the membrane tension read

$$N_s^{a\,j} = N_\varphi^{a\,j} = \frac{1}{2}\,e^j\,\zeta^j \Delta\mu\,. \tag{S32}$$

2.4 Cytoplasmic pressure

From the continuous constitutive relation (Eq. 4 in the main text), we can express the uniform cytoplasmic pressure by summing discrete enclosed volume contributions in Eq. S24

$$P = -K\left(\sum V(\mathbf{x}_i, \mathbf{x}_{i+1}) - \mathcal{V}_0\right)\,. \tag{S33}$$

2.5 Balance of forces

The membrane stress is described by a tensor living on segments

$$\mathbf{N}^j = N_s^j\,\mathbf{t}^j \otimes \mathbf{t}^j + N_\varphi^j\,\mathbf{e}_\varphi \otimes \mathbf{e}_\varphi\,, \tag{S34}$$

where $\mathbf{t}^j$ is the unit tangent vector associated to the segment j.

The principle of virtual work (Eq. S21) provides a natural way for discretizing the equations of motion: for any virtual motion of the vertices $(\hat{\mathbf{x}}_i)_{0\le i\le n+1}$,

$$\sum_{\text{vert } i} P\,\mathbf{g}_i \cdot \hat{\mathbf{x}}_i - \sum_{\text{seg } j}\left(N_s^j\,\hat{d}_s^j + N_\varphi^j\,\hat{d}_\varphi^j\right) A^j = 0\,, \tag{S35}$$

where P is the cytoplasmic pressure defined in Eq. S33, the virtual work of which is derived from the continuous formulation (Eq. S21): $P\,\hat{\dot{\mathcal{V}}} = P\,\nabla_{\mathbf{x}_i}\mathcal{V}\cdot\hat{\dot{\mathbf{x}}}_i = P\,\mathbf{g}_i\cdot\hat{\dot{\mathbf{x}}}_i$. The virtual strain rates read, in analogy with equation (S30),

$$\hat{d}_s^j = \frac{\mathbf{t}^j\cdot(\hat{\dot{\mathbf{x}}}_{j+1}-\hat{\dot{\mathbf{x}}}_j)}{\ell^j} \tag{S36a}$$

$$\hat{d}_\varphi^j = \frac{\mathbf{e}_r\cdot(\hat{\dot{\mathbf{x}}}_j+\hat{\dot{\mathbf{x}}}_{j+1})}{r_j+r_{j+1}} \tag{S36b}$$

When the virtual velocities are eliminated, Eq. S35 yields a set of $2n$ equations for the $2n$ degrees of freedom of the system. These equations depend on the velocities through the constitutive laws.

2.6 Membrane incompressibility with turnover dynamics

Each segment carries a volume $w^j(t)$, which evolves in analogy with the continuous formulation (Eq. S20):

$$\dot{w}^j = -k_d\,w^j + v_p\,A^j\,, \tag{S37}$$

where A^j is the lateral areal defined in Eq. S28.

This volume is used to reconstruct the thickness of a segment, based on the position of its end vertices:

$$e^j = \frac{w^j}{A^j}\,. \tag{S38}$$

3 Numerical implementation

3.1 Numerical code

We adapted to axisymmetric membranes a preexisting C++ code called *DVR* (Discrete Viscous Rods), originally developped for simulating the dynamics of viscous threads (10). We implemented the discrete axisymmetric geometrical relations Eq. S23 to Eq. S31, active (Eq. S32) and cytoplasmic (Eq. S33) forces, and segment volume update (Eq. S37).

3.2 Remeshing: adaptive refinement and coarsening

Gradients of active tension trigger membrane flows and rapid accumulation of Lagrangian points toward the equatorial region, where the contractile activity is maximum, and to the depletion from regions of lowest activity. Refinement is also needed due to the large curvature in the equatorial furrow. We implemented both mesh adaptation and coarsening as follows.

Adaptive mesh refinement The procedure used for axisymmetric membranes is very similar to the original mesh refinement algorithm implemented in the *DVR* code (10). Segments that need refinement are first identified at the end of a viscous time-step. The criterion is based on the comparison of the length of the segment to some prescribed maximal length, which has been chosen as $1.5\,\ell_0$ where $\ell_0 = 2\pi R_0/n_0$ is the initial length of segments (n_0 is the initial the number of segments). This refinement criterion has been adjusted manually to offer the best compromise between accuracy and efficiency. A new vertex is inserted in between the two vertices of each segment that have been marked, and two new segments are allocated to replace the former one. The new vertex is inserted, two new segments are allocated and the former segment is removed. The new vertex position and velocity are calculated by an interpolation of order 2 of position and velocity of its neighboring vertices. The stretching forces which depend on the derivatives of the positions and velocities to an order up to two, remain hence smooth upon subdivision. The volume of the two new segments is finally interpolated to globally conserve volume and to result in the same membrane thickness.

Adaptive mesh coarsening The mesh coarsening procedure has been developed specifically for the present application. It follows the same lines as the previous conventional mesh refinement algorithm. At the end of a viscous time-step, the smallest segment is sought. Coarsening is applied to it when its length is below a prescribed threshold, or when the angle between its neighboring segments exceeds a threshold. This criterion triggers coarsening in the presence of large stretch, or when the curvature is large. Coarsening is applied by removing this segment and its two adjacent vertices, and replacing them by a single vertex. The position and velocity of this new vertex is interpolated again up to order 2, and the volume of the two adjacent segments are updated to conserve volume globally.

3.3 Validation: spherical contraction under uniform active tension

Analytical solution We consider a spherical isotropic active membrane enclosing a compressible fluid. Its initial radius is R_0 and the membrane shell has an initial thickness e_0. At time $t = 0$ we apply an isotropic active tension N_0^a, and consider the spherical contraction, prescribed in spherical coordinates as

$$R(\theta_0, \varphi_0, t) = R(t) \tag{S39}$$
$$\theta(\theta_0, \varphi_0, t) = \theta_0 \tag{S40}$$
$$\varphi(\theta_0, \varphi_0, t) = \varphi_0 \tag{S41}$$

Membrane volume dynamics with turnover (Eq. S20) reads

$$2\frac{\dot{R}}{R} + \frac{\dot{e}}{e} = -k_d + \frac{v_p}{e} \tag{S42}$$

The strain rate tensor is locally isotropic,

$$\mathbf{d} = \frac{\dot{R}(t)}{R(t)} \left(\mathbf{e}_s \otimes \mathbf{e}_s + \mathbf{e}_\varphi \otimes \mathbf{e}_\varphi\right). \tag{S43}$$

and so is the membrane tension tensor,

$$\mathbf{N} = \left(N^v + N^a\right) \left(\mathbf{e}_s \otimes \mathbf{e}_s + \mathbf{e}_\varphi \otimes \mathbf{e}_\varphi\right). \tag{S44}$$

The viscous part is given by the constitutive law in Eq. S14 as

$$N^v = 6\,\eta\, e(t)\, \frac{\dot{R}(t)}{R(t)} \tag{S45}$$

and the active part is prescribed as a function $N^a(t)$.

The constitutive law for the inner compressible fluid reads

$$P = -K \left(\frac{4\,\pi}{3}\, R^3(t) - V_0\right) \tag{S46}$$

From the weak formulation of equilibrium (Eq. S21), balance of forces reads

$$P = \frac{2}{R(t)}\, N_0^a \tag{S47}$$

Combining the previous equations we get a system of two coupled ordinary differential equations (o.d.e.) governing the time evolution of the radius and the thickness

$$N_v + N_a^0 = 6\,\eta\, e(t)\, \frac{\dot{R}(t)}{R(t)} + N_0^a = -K \frac{R(t)}{2} \left(\frac{4\,\pi}{3}\, R^3(t) - V_0\right) \tag{S48a}$$
$$2\frac{\dot{R}(t)}{R(t)} + \frac{\dot{e}(t)}{e(t)} = -k_\mathrm{d} + \frac{v_\mathrm{p}}{e(t)} \tag{S48b}$$

Validation procedure We validate our implementation of the compressible cytoplasm and of turnover by comparing a numerical solution to the ordinary differential equations in Eq. S48 obtained using Mathematica® 9.0.1., to the results of the simulation. We plot a comparison of numerical and analytical results for various values of K at fixed turnover in Fig. S6 *A* and for various $k_\mathrm{d} > 0$ and $v_\mathrm{p} > 0$ at fixed K in Fig. S6 *B* (see Figures).

3.4 Stability

A dimension analysis of the problem leads to three typical time-scales:

- An active time-scale
$$T_a = \frac{e_0 \eta}{N_0^a} = \frac{2\eta}{\zeta_0 \Delta\mu}\,, \tag{S49}$$
that characterizes the typical time for viscous deformation of the actomyosin gel submitted to a basal active stress $\zeta_0\Delta\mu/2$. For any activity ζ, one can define a corresponding active time scale $T_a(\zeta) = 2\eta/\zeta\Delta\mu$. T_a is therefore the longest active time-scale in our problem, since from Eq. 2 of the main text $\zeta(S,t) \geq \zeta_0$.

- A cytoplasmic compressibility time-scale
$$T_K = \frac{\eta\, e_0}{R_0 V_0 K}\,, \tag{S50}$$
that compares the cortex deformation time scale to the cytoplasmic pressure response.

- A turnover time-scale
$$\frac{1}{k_d}\,, \tag{S51}$$
that characterizes the typical time for the layer thickness relaxation.

Active layer intrinsic instability
We first compare the turnover and active time-scales. An active viscous layer with variable thickness is intrinsically unstable without turnover: any spatial difference in thickness creates a tension gradient that triggers an active flow toward the regions of higher thickness. The thickness increase enhances the gradient of tension and therefore amplifies itself via the cortical flow. Turnover stabilizes this effect if thicker regions depolymerize rapidly enough and thinner regions regrow rapidly enough. The active layer remains therefore stable if $T_a\, k_d \gg 1$.

Compressibility time-scale
We compare the compressibility time-scale T_K to the active time-scale T_a. The ratio $\frac{T_K}{T_a} = \frac{e_0}{R_0}\frac{\zeta_0\Delta\mu}{V_0 K}$ compares active tension of the layer and cytoplasmic pressure. To avoid collapse of the membrane it has therefore to be lower than one.

Code general stability
The time-step has to be smaller than all other time-scales in the problem. Taking into account the previous stability requirements we end up with the following global requirement for code stability
$$dt \ll T_K < \frac{1}{k_d} \ll T_a\,. \tag{S52}$$

3.5 Choice of numerical parameters

The values of numerical parameters are chosen relatively to a scale of reference. We naturally choose the initial cell radius R_0 as length-scale of reference, and the active time at poles $T_a = \frac{2\eta}{\zeta_0\Delta\mu}$ as the time-scale of reference. We pick realistic estimates of the relative numerical parameters from various references as summarized in Table S1. We summarize in Table S2 all the sets of numerical parameters used for generating the figures and movies in this paper.

4 Scaling model

We detail here the calculations of the scaling model on the minimal geometry sketched in Fig. 6 *A* (Main Text).

4.1 Static analysis

Cytoplasmic volume conservation imposes a relation between the pole radius R and the initial cell size R_0 of the form

$$R_0^3 = R^3 \left[1 + \frac{3}{2}\cos\theta - \frac{1}{2}\cos^3\theta\right] \equiv R^3 F(\theta) \tag{S53}$$

In Fig. 6 *B*, the disappearance of the local minimum $\theta > 0$ in the energy $\mathcal{E}/\mathcal{E}_0$ when κ is increased above some threshold defines a critical point (κ_c, θ_c). This critical point, where the final cell jumps from an incomplete constriction to a full division, is given by

$$0 = \left.\frac{\partial \mathcal{E}}{\partial \theta}\right|_{\theta_c}, \qquad 0 = \left.\frac{\partial^2 \mathcal{E}}{\partial \theta^2}\right|_{\theta_c}. \tag{S54}$$

Using Mathematica® 9.0.1 we solve this system of equations and get the following numerical values for complete constriction threshold $\kappa_c \approx 0.4053$, corresponding to a constriction state $\theta_c \approx 46.46°$ or equivalently $r_{f_c} = 0.5884\, R_0$.

4.2 Dynamics

We evaluate the power dissipated by viscous effects as defined in Eq. 9 in the main text. After calculation it reads

$$\mathcal{P}_\mathrm{d} = 4\pi e_0\, \eta \left(\frac{dr_f}{dt}\right)^2 \left[(1+\cos\theta) + \lambda \frac{F(\theta)^{1/3}}{\sin\theta}\right], \tag{S55}$$

where we defined the parameter

$$\lambda \equiv \frac{w}{2R_0}\frac{e_f}{e_0}. \tag{S56}$$

We calculate the time variation of the mechanical energy $\frac{d\mathcal{E}}{dt} = -\mathcal{P}_d$ rescaled by $\mathcal{E}_0$:

$$\begin{aligned}
\frac{1}{\mathcal{E}_0}\frac{d\mathcal{E}}{dt} &= \frac{\partial \mathcal{E}/\mathcal{E}_0}{\partial \theta}\frac{\partial \theta}{\partial r_f}\frac{dr_f}{dt} \\
&= -\frac{\mathcal{P}_\mathrm{d}}{\mathcal{E}_0} \\
&= -\frac{T_a}{R_0^2}\left(\frac{dr_f}{dt}\right)^2 \left[(1+\cos\theta) + \lambda \frac{F(\theta)^{1/3}}{\sin\theta}\right],
\end{aligned}$$

with $T_a = \frac{\eta e_0}{N_0^a}$ as in the continuous formulation. It leads to

$$\begin{aligned}
\frac{T_a}{R_0}\frac{dr_f}{dt} &= -\frac{\partial \mathcal{E}/\mathcal{E}_0}{\partial \theta}\left(\frac{\partial r_f/R_0}{\partial \theta}\right)^{-1} \left[(1+\cos\theta) + \lambda \frac{F(\theta)^{1/3}}{\sin\theta}\right]^{-1} \\
&\equiv -\mathcal{H}(\theta, \kappa, \lambda).
\end{aligned} \tag{S57}$$

Since $\mathcal{E}/\mathcal{E}_0$ depends only on θ and κ according to equation (9) in the main text, the rate of constriction reduces to a simple function $\mathcal{H}$ of θ, κ and λ only. One can solve for the radius of the contractile ring as a function of time for given values of κ and λ by inserting $r_f/R_0 = \sin\theta\, F(\theta)^{-1/3}$ in Eq. S57, integrating numerically the non-linear differential equation for $\theta(t)$ and recalculating $r_f(\theta(t))$.

One should note that κ and λ are not independent in the continuous model. In particular $\lambda \propto \frac{e_f}{e_0}$ should increase with $\kappa \propto N_f^a - N_0^a$ at fixed turnover because of increased cortical flows that we neglected here. Conversely, κ depends on the ratio e_f/e_0 as we show using the continuous expressions for active tensions:

$$\begin{aligned} \kappa &\approx \frac{w}{2R_0}\frac{N_f^a - N_0^a}{N_0^a}, \\ &\approx \frac{w}{2R_0}\left(\frac{\zeta_f}{\zeta_0}\frac{e_f}{e_0} - 1\right), \end{aligned} \tag{S58}$$

where ζ_f and ζ_0 are the activities respectively in the furrow and at poles.

We solve numerically Eq. S57 with Mathematica® 9.0.1., varying the activity in the furrow ζ_f/ζ_0 or its width w/R_0 to mimick the RhoA-GTP signal and the furrow thickness e_f/e_0 to mimick the effect of turnover. Results are plotted in Fig. 7 (Main text).

SUPPORTING REFERENCES

1. Yeung, A., and E. Evans. 1989. Cortical shell-liquid core model for passive flow of liquid-like spherical cells into micropipets. *Biophys. J.*, 56(1):139–49.

2. Daniels, B.R., B.C. Masi, and D. Wirtz. 2006. Probing single-cell micromechanics in vivo: the microrheology of C. elegans developing embryos. *Biophys. J.* 90(12):4712–4719.

3. Charras, G.T., T.J. Mitchison, and L. Mahadevan. 2009. Animal cell hydraulics. *J. Cell Sci.* 122(18):3233–3241.

4. Kalwarczyk, T., N. Zie, R. Hozyst, and C.S. Wyszy. 2011. Comparative Analysis of Viscosity of Complex Liquids and Cytoplasm. *Nano Lett.* 11(5):2157–2163.

5. Zhang, W., and D.N. Robinson. 2005. Balance of actively generated contractile and resistive forces controls cytokinesis dynamics *Proc. Natl. Acad. Sci. USA* 102(20):7186–7191.

6. Mayer, M., M. Depken, J.S. Bois, F. Julicher, and S.W. Grill. 2010. Anisotropies in cortical tension reveal the physical basis of polarizing cortical flows. *Nature* 467(7315):617–21.

7. Spek, J. 1918. Oberflchenspannungsdifferenzen als eine Ursache der Zellteilung. *Archiv fr Entwicklungsmechanik der Organismen* 44(1):5–113.

8. Dan, K., T. Yanagita, and M. Sugiyama. 1937. Behavior of the cell surface during cleavage. I. *Protoplasma* 28(1):66–81.

9. Hiramoto, Y. 1958. A quantitative description of protoplasmic sea-urchin egg. *The Journal of Experimental Biology* 35(2):407–424.

10. Audoly, B., N. Clauvelin, P-T. Brun, M. Bergou, E. Grinspun, and M. Wardetzky. 2013. A discrete geometric approach for simulating the dynamics of thin viscous threads. *J. Comput. Phys.* 253:18-49 (in press doi:10.1016/j.jcp.2013.06.034).

11. Green, A.E., and W. Zerna. 2002. *Theoretical Elasticity*, Dover Publications, pp. 386–389.New-York, 386-389.

12. Salbreux, G., J. Prost, J-F. Joanny. 2009. Hydrodynamics of Cellular Cortical Flows and the Formation of Contractile Rings. *Phys. Rev. Lett.* 103(5):058102.

13. Kruse, K., J-F. Joanny, F. Julicher, J. Prost, and K. Sekimoto. 2005. Generic theory of active polar gels : a paradigm for cytoskeletal dynamics. *Eur. Phys. J. E Soft Matter* 16(1):5–16.

14. Happel, J., and H. Brenner. 1983. *Low Reynolds Number Hydrodynamics*, Kluwer Academic Publishers, Norwell.

15. Libai, A., and J.G. Simmonds. 1995. *The Nonlinear Theory of Elastic Shells*, Cambridge University Press, Cambridge.

16. Bement, W.M., H. Benink, and G. von Dassow. 2005. A microtubule-dependent zone of active RhoA during cleavage plane specification. *J. Cell Biol.* 170(1):91–101.

17. Von Dassow, G., K.J.C Verbrugghe, A.L. Miller, J.R. Sider, and W.M. Bement. 2009. Action at a distance during cytokinesis. *J. Cell Biol.* 187(6):831–845.

18. Tinevez, J.Y., U. Schulze, G. Salbreux, J. Roensch, J-F. Joanny, and E. Paluch. 2009. Role of cortical tension in bleb growth. *Proc. Natl. Acad. Sci. USA* 106(44):18581-18586.

19. Guha, M., M. Zhou, and Y. Wang. 2005. Cortical Actin Turnover During Cytokinesis Requires Myosin II. *Curr. Biol.* 15(8):732–736.

20. Murthy, K., and P. Wadsworth. 2005. Myosin-II-dependent Localization and Dynamics of F-actin During Cytokinesis. *Curr. Biol.* 15(8):724–731.

21. Fritzsche, M., A. Lewalle, T. Duke, K. Kruse, and G. Charras. 2013. Analysis of Turnover Dynamics of the Submembranous Actin Cortex. *Mol. Biol. Cell* 24:757–767.

22. Salbreux, G., G. Charras, and E. Paluch. 2012. Actin Cortex Mechanics and Cellular Morphogenesis. *Trends Cell Biol.* 22(10):536–545.

23. Clark, A.G., K. Dierkes, and E.K. Paluch. 2013. Monitoring Actin Cortex Thickness in Live Cells. *Biophys. J.* 105(3):570–580.

24. Argiros, H., L. Henson, C. Holguin, V. Foe, and C.B. Shuster. 2012. Centralspindlin and chromosomal passenger complex behavior during normal and Rappaport furrow specification in echinoderm embryos. *Cytoskeleton (Hoboken)* 69(10):840-853.

SUPPORTING TABLES

Notation	Quantity	Experimental value(s)	Numerical value(s)	Ref(s).
R_0	Animal cell radius	$10 - 100\ \mu m$	1	(16, 17)
e_0	Cortical thickness	$0.2 - 2\ \mu m$	0.02	(22, 23)
w	RhoA-GTP equatorial signal width	$1 - 10\ \mu m$	0.1	(16, 17)
$1/2\,\zeta_0 \Delta\mu$	Basal cortical active stress	$10^3\ Pa$	1	(18)
T_a	Typical cytokinesis time-scale	$10^3\ s$	10	(16, 17)
$\eta\ = 1/2\,\zeta_0 \Delta\mu\, T_a$	Actomyosin viscosity	$10^6\ Pa\,s$	10	/
$k_{\rm d}\ = \log 2/\tau_{\rm FRAP}^{1/2}$	Depolymerization rate	$0.04\ s^{-1}$	4	(19–21)
$v_{\rm p} = e_0\, k_{\rm d}$	Polymerization velocity	$0.008 - 0.08\ \mu m\, s^{-1}$	0.08	/

TABLE S1: Notations used in the main and supporting texts and their typical experimental and numerical value(s) with reference(s). Numerical values have been chosen so that $R_0 = 1$ and $T_a = 10$ are the length and time-scales of reference.

Figure(s) and movie(s)	**Radius** R_0	**Signal amplitude** $\delta\zeta^\infty$	**Signal width** w/R_0	**Depol. rate** $k_d\, T_a$	**Bulk mod.** K
Figs. 1, 2 Figs. S2, S3, S4, S5 Movies S1, S3, S5 and S2(Right)	1	75	0.1	40	250
Figs. 3 *A*, 3 *B(Inset)* MovieS2 *(Left)*	1	❶: 10 ❷: 25 ❸: 40 ❹: 50 ❺: 75 ❻: 100 MovieS2*(L)*: 25	0.1	40	250
Fig. 3 *B (diagram)*	1	0 to 81 by 1	0.1	40	250
Fig. 4 MovieS4	1	75	0.1	①: 30 ②: 40 ③: 80	250
Fig. 5	(a): 0.5 (b): 1 (c): 2 (d): 4	75	(a): 0.1 (b): 0.2 (c): 0.3 (d): 0.4	40	250

TABLE S2: Numerical parameters used for generating the main text and supporting figures and movies (except for code validation, see Figs. S7A and B). The absolute or relative value of following parameters remain unchanged: $e_0/R_0 = 0.02$, $v_p = e_0\, k_d$, $n_0 = 501$.

SUPPORTING FIGURES

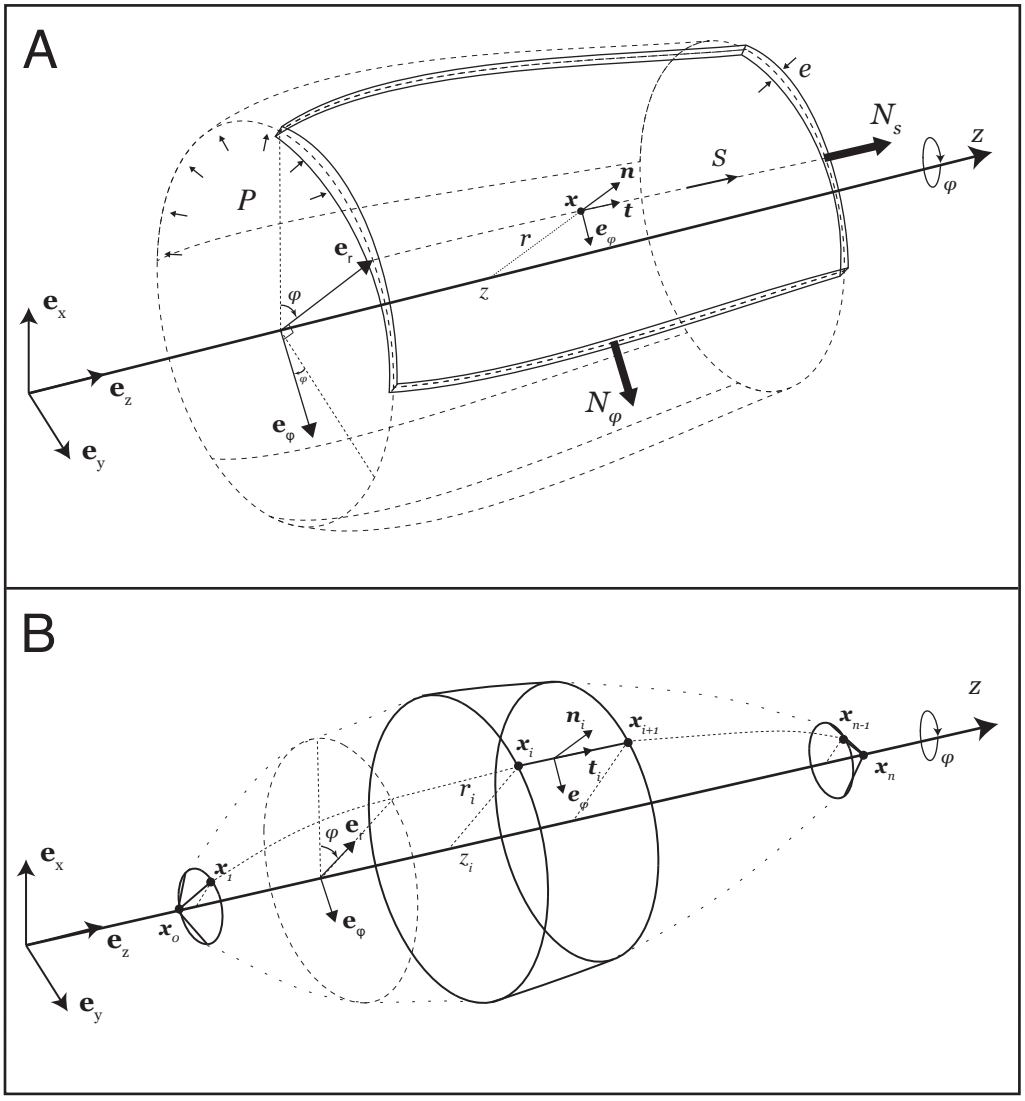

FIGURE S1: Sketch of the continuous and discrete axisymmetric membrane shell: *(A)* Piece of the membrane layer of thickness e. The membrane midline is parametrized by $(r(S), z(S))$ in the plane $(\mathbf{e}_z, \mathbf{e}_r)$. In the local Frenet frame $\{\mathbf{t}(S), \mathbf{n}(S), \mathbf{e}_\varphi\}$, the membrane is submitted to a tension N_s in its axial direction $\mathbf{t}$, to a tension N_φ in its azimuthal direction $\mathbf{e}_\varphi$ and to a uniform pressure P in its normal direction $\mathbf{n}$. *(B)* Discrete axisymmetric membrane midsurface reconstructed by revolving the discrete midline $\{\mathbf{x}_i = (z_i, r_i)\}_{0 \leq i \leq n+1}$ defined in the plane $(\mathbf{e}_z, \mathbf{e}_r)$.

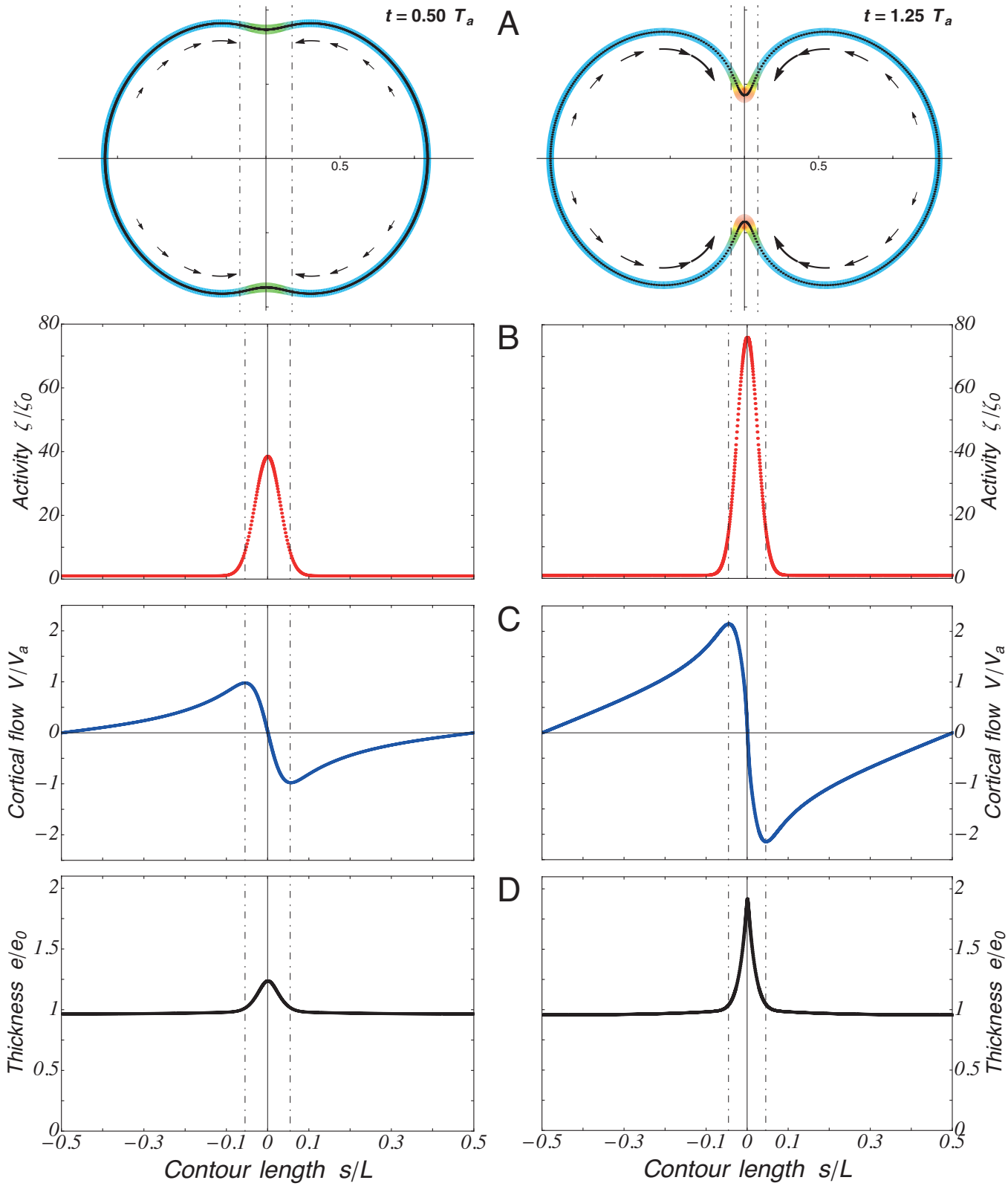

FIGURE S2: Cortical flow, furrow region and thickness: *(A)* Cell cortex shape and thickness at times $t = 0.5\,T_a$ (left) and $t = 1.25\,T_a$ (right). *(B, C and D)* Corresponding plots of, respectively, activity signal ζ/ζ_0, cortical flow velocity V/V_a ($V_a = R_0/T_a$) and thickness e/e_0 along the midline contour length s/L. The cortical flow is oriented toward the furrow region and its amplitude increases with the equatorial signal between $t = 0.5\,T_a$ *(left)* and $t = 1.25\,T_a$ *(right)*. Its extrema delimit the furrow region, demarcated by the two dot-dashed vertical lines in each figure. The increase of the cortical flow triggers a greater accumulation of actomyosin in the furrow region, leading to an expansion of its thickness.

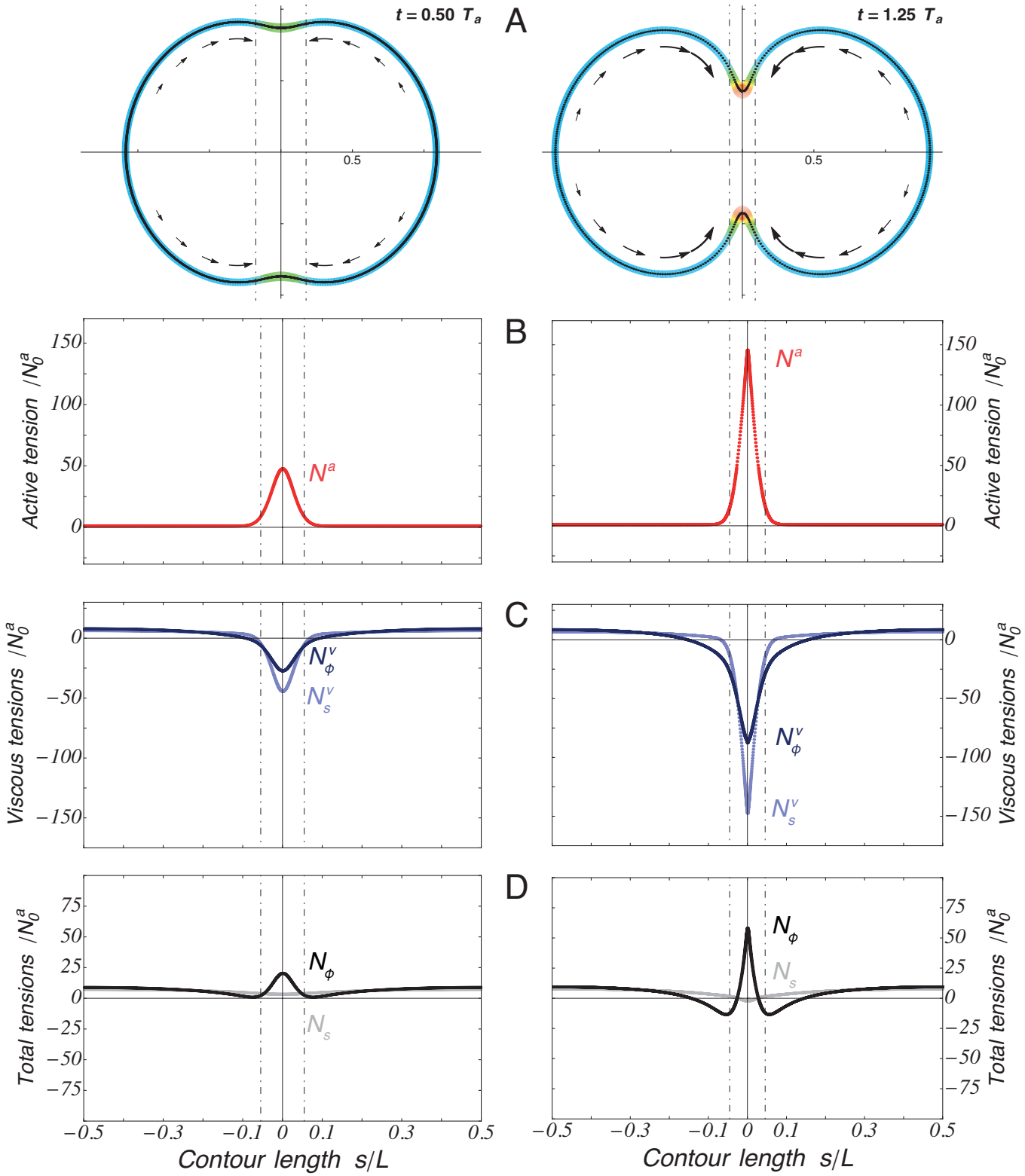

FIGURE S3: Cortical tensions: *(A)* Cell cortex shape and thickness at times $t = 0.5\,T_a$ *(left)* and $t = 1.25\,T_a$ *(right)*. *(B, C and D)* Corresponding plots of, respectively, the active tension N^a, the viscous tensions N_s^v, N_φ^v and the total tensions N_s, N_φ in the membrane, rescaled by the basal active tension N_0^a. The active tension is isotropic in the axial and azimuthal directions whereas the viscous tensions are appreciably anisotropic near the furrow region, delimited by dot-dashed vertical lines. It leads to total membrane tensions that are globally anisotropic: the azimuthal tension is markedly greater than the axial tension in the furrow region leading to a furrow line tension that constricts the cell, whereas the regions bordering the furrow are more stretched in their axial direction leading to non-sperical shapes.

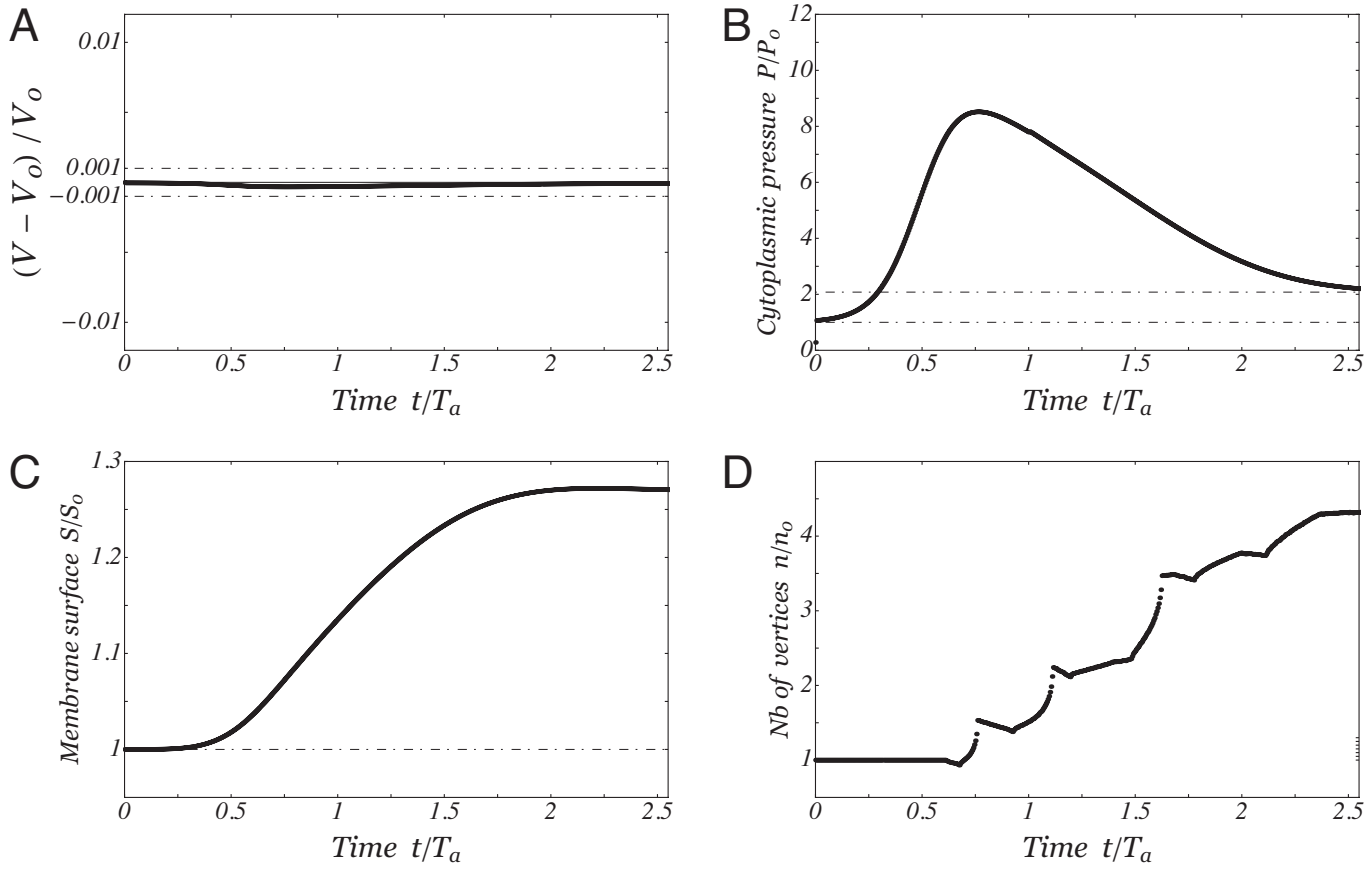

FIGURE S4: Cytoplasmic volume conservation and pressure, membrane surface and number of vertices for the first simulation (Fig. 1, Movies S1 and S5): *(A)* Plot of the cytoplasmic volume variation $(V-V_0)/V_0$ over time. We added two horizontal lines to show that the error is below 0.1%. *(B)* Cytoplasmic pressure P rescaled by the initial Laplace pressure $P_0 = 2N_0^a/R_0$. The cytoplasmic pressure increases rapidly during the transient phase and then decreases slowly toward a value roughly two times greater than the initial pressure. *(C)* Time evolution of the membrane surface S rescaled by the initial surface $S_0 = 4\pi R_0^2$. *(D)* Time evolution of the number of vertices n, rescaled by its initial value n_0, as a result of the two adaptive remeshing procedures: refinement and coarsening.

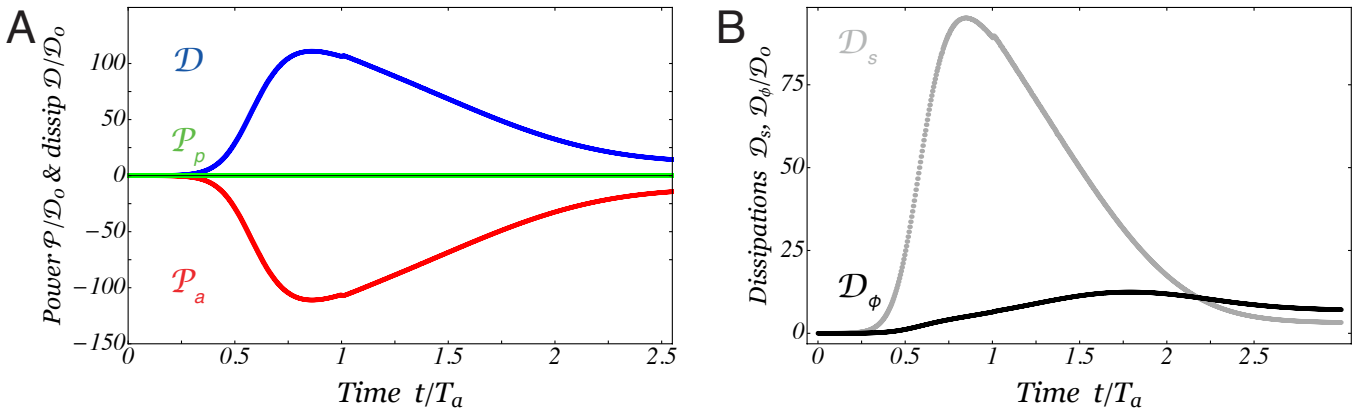

FIGURE S5: Active and dissipated power for the first simulation (Fig. 1, Movies S1 and S5): *(A)* Plot of the time evolution of the total dissipation $\mathcal{D}$, of the work of active forces $\mathcal{P}_a$ in the membrane and of the work of cytoplasmic pressure $\mathcal{P}_p$ rescaled by $\mathcal{D}_0 = 4\pi R_0^2 N_0^a / e_0 \eta$. We make the cytoplasm almost incompressible by assigning a high value of its bulk modulus $K = 250$. As a result it does not store any elastic energy and its work remains null. The work of active forces $\mathcal{P}_a$ in the membrane is therefore fully dissipated by viscous effects $\mathcal{D}$. The work of active forces increases in the transient regime and then decreases almost linearly in time and finally relaxes exponentially towards a plateau above 0. We find again the successive phases of constriction described in Fig. 2 (Main text) and we confirm that maintaining a signal at equator sustains a cortical flow after constriction completion that maintains dissipation non-zero. *(B)* Plot of the time evolution of axial and azimuthal components $\mathcal{D}_s$ and $\mathcal{D}_\varphi$ of the viscous dissipation. The axial components reveals the dissipation due to cortical flows whereas the azimuthal component is essentially due to the furrow constriction. We observe that most of the dissipation comes from cortical flows occuring from the poles to the equator, except in the last phase of constriction for $t/T_a \gtrsim 2.5$ where the cortical flows decrease significantly.

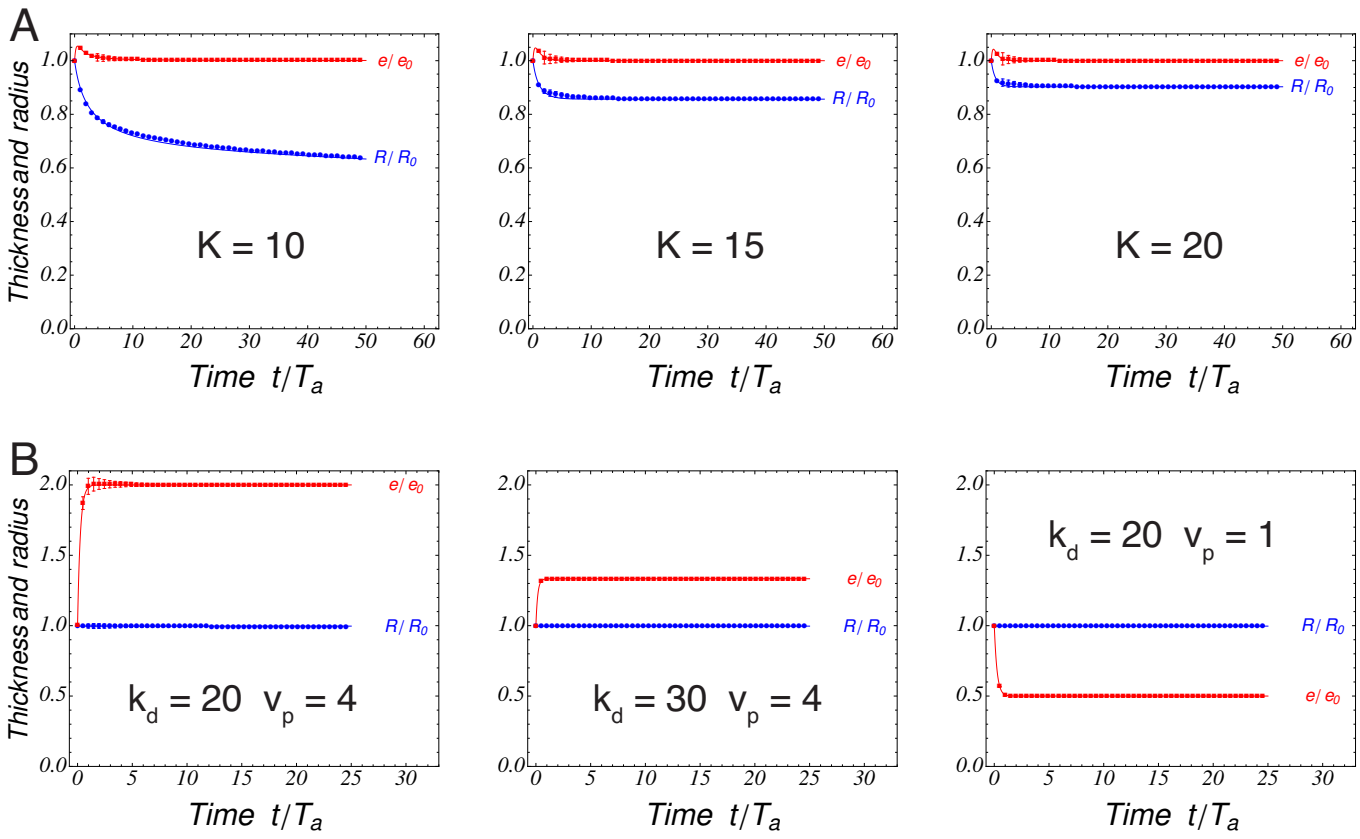

FIGURE S6: Code validation: spherical contraction under uniform active tension. Lines are solutions of the analytical equations for the cell radius R and membrane thickness e. Markers are solutions of the numerical model and error bars indicate maximum deviations along the membrane from the mean value. *(A)* Validation of the compressible cytoplasm implementation for three low values of the bulk modulus $K = 10$, 15 and 20 ($k_d = 40$ and $v_p = e_0\, k_d = 0.1$). The cell radius contracts correctly under the effect of active tension and shows little longitudinal error. The amplitude of the contraction decreases when K increases as expected. The membrane thickness reaches rapidly its stationnary value v_p/k_d. *(B)* Validation of the turnover implementation for three values of the depolymerization rate k_d and polymerization velocity v_p, so that the initial membrane thickness $e_0 = 0.1$ is different from v_p/k_d. A high value of the bulk modulus $K = 250$ maintains the cell radius R at its initial value R_0 to conserve cytoplasmic volume. In each case, the membrane thickness e reaches its stationnary value v_p/k_d according to the analytical prediction and shows little error along the membrane.

SUPPORTING MOVIES

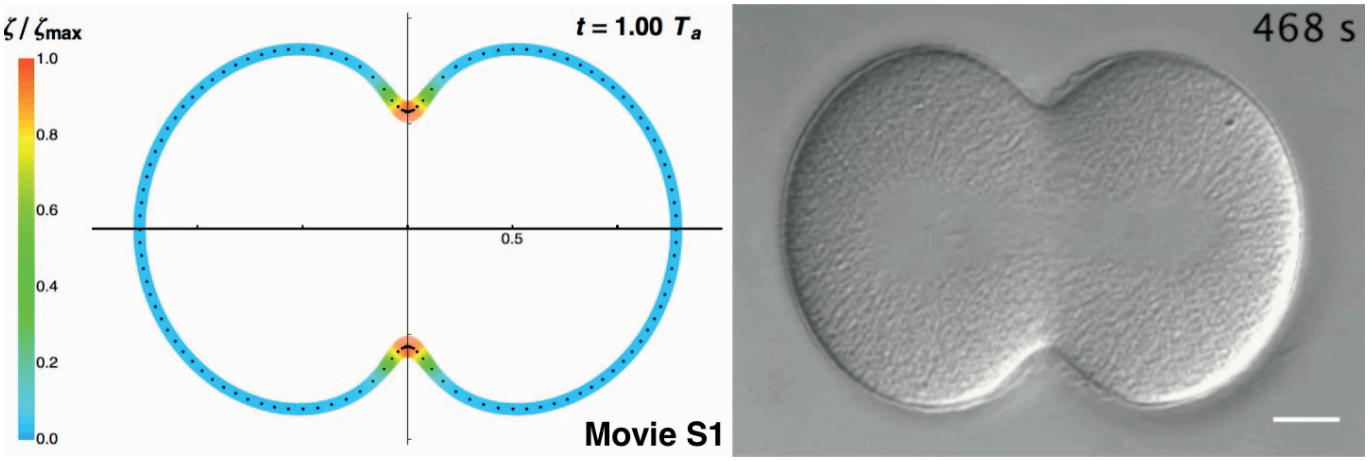

MOVIE S1: *(Left)* Dynamics of the cell shape and cortex thickness corresponding to Fig. 1 (Main text) in a section plane $(\mathbf{e}_z, \mathbf{e}_r)$, in response to the rescaled activity signal $\zeta/\zeta_{\max}$, illustrated by the color shading. A few Lagrangian points are represented within the membrane to capture the cortical flows. *(Right)* DIC microscopy images of a sand-dollar zygote (dendraster) deprived of its hyaline layer and jelly coat under cytokinesis. The cell is not flattened and scale bar is $20\mu m$. (Credits: G. Von Dassow). Numerical and experimental movies have been synchronized by rescaling the active time scale to $T_a = 468s$.

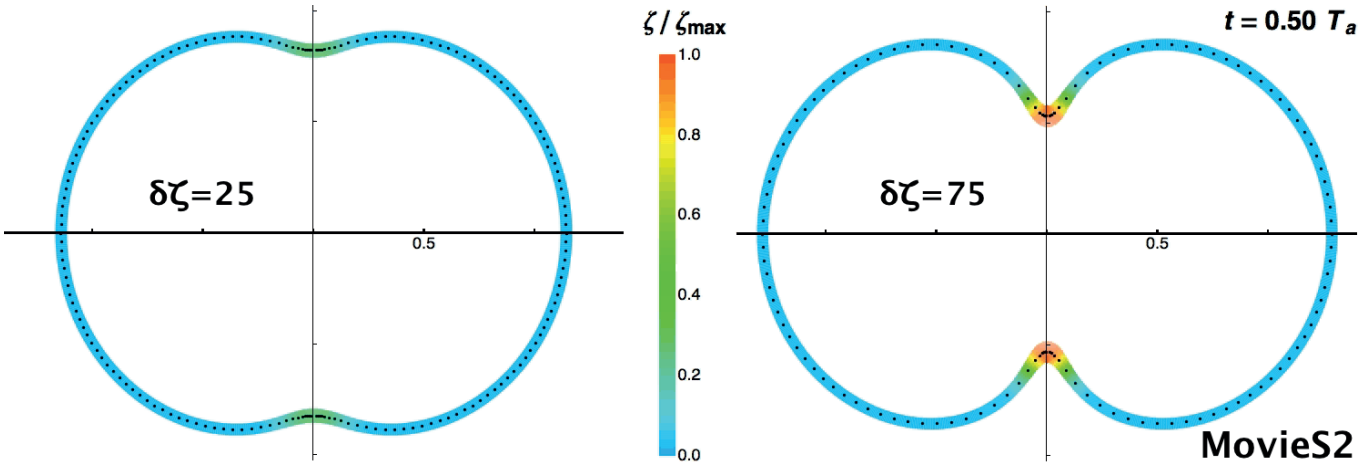

MOVIE S2: Comparison of the cell shape and cortex thickness dynamics in a section plane $(\mathbf{e}_z, \mathbf{e}_r)$ for the two equatorial signal amplitude $\delta\zeta^\infty = 25$, and $\delta\zeta^\infty = 75$, corresponding respectively to the furrow radius time evolutions ❷ and ❺ in Fig. 3 *B*. A few Lagrangian points are represented within the membrane to capture the cortical flows

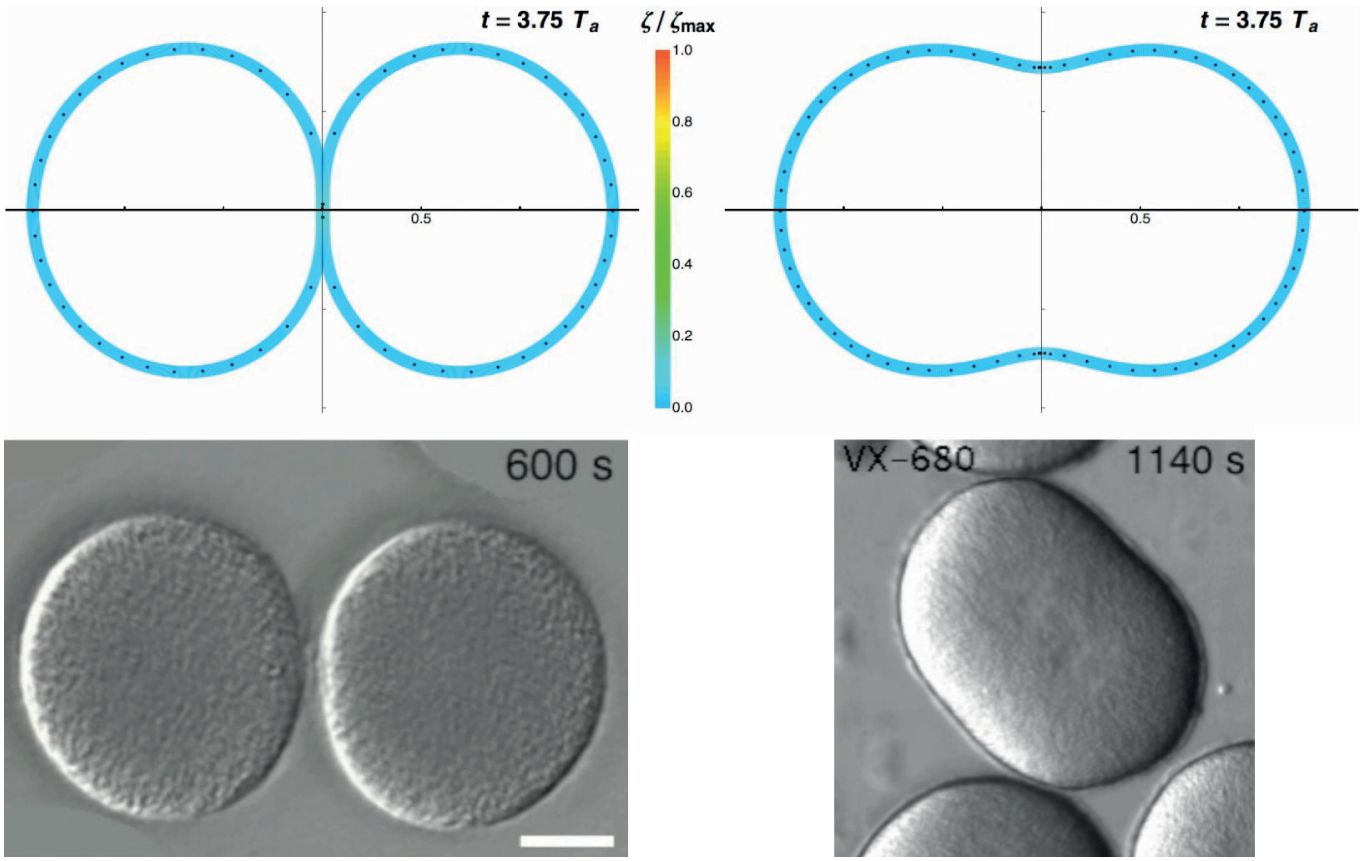

MOVIE S3: Illustration of the hysteretic behavior. ***NUMERICS (Top)*** Dynamics of the cell shape and cortex in a section plane $(\mathbf{e}_z, \mathbf{e}_r)$ when the signal is decreased down to a value smaller than the threshold : *(Top Left)* after constriction completion or *(Top Right)* prematurely before the critical ingression radius $r_f \approx 0.6$ has been reached. ***EXPERIMENTS (Bottom)*** Qualitative comparison with the furrow constriction dynamics in sea-urchin eggs. *(Bottom Left)* Non-compressed S. purpuratus eggs in calcium-free artificial seawater and deprived of its hyaline layer (DIC microscopy, scale bar is $20\mu m$, credits: G. Von Dassow). The rounding up of cells at the end of furrow constriction (without cell adhesion) may be attributed to a decrease of the equatorial signal according to numerical results above. The divided state remains mechanically stable. *(Bottom Right)* L. pictus egg deprived of its enveloppe and cultured in natural seawater with 50 mM VX-680 (24) (DIC microscopy, credits: C. Bradley Shuster). The regression of the furrow, which leads to a binucleated cell, may be attributed to a premature decrease of equatorial contracility according to numerical results above.

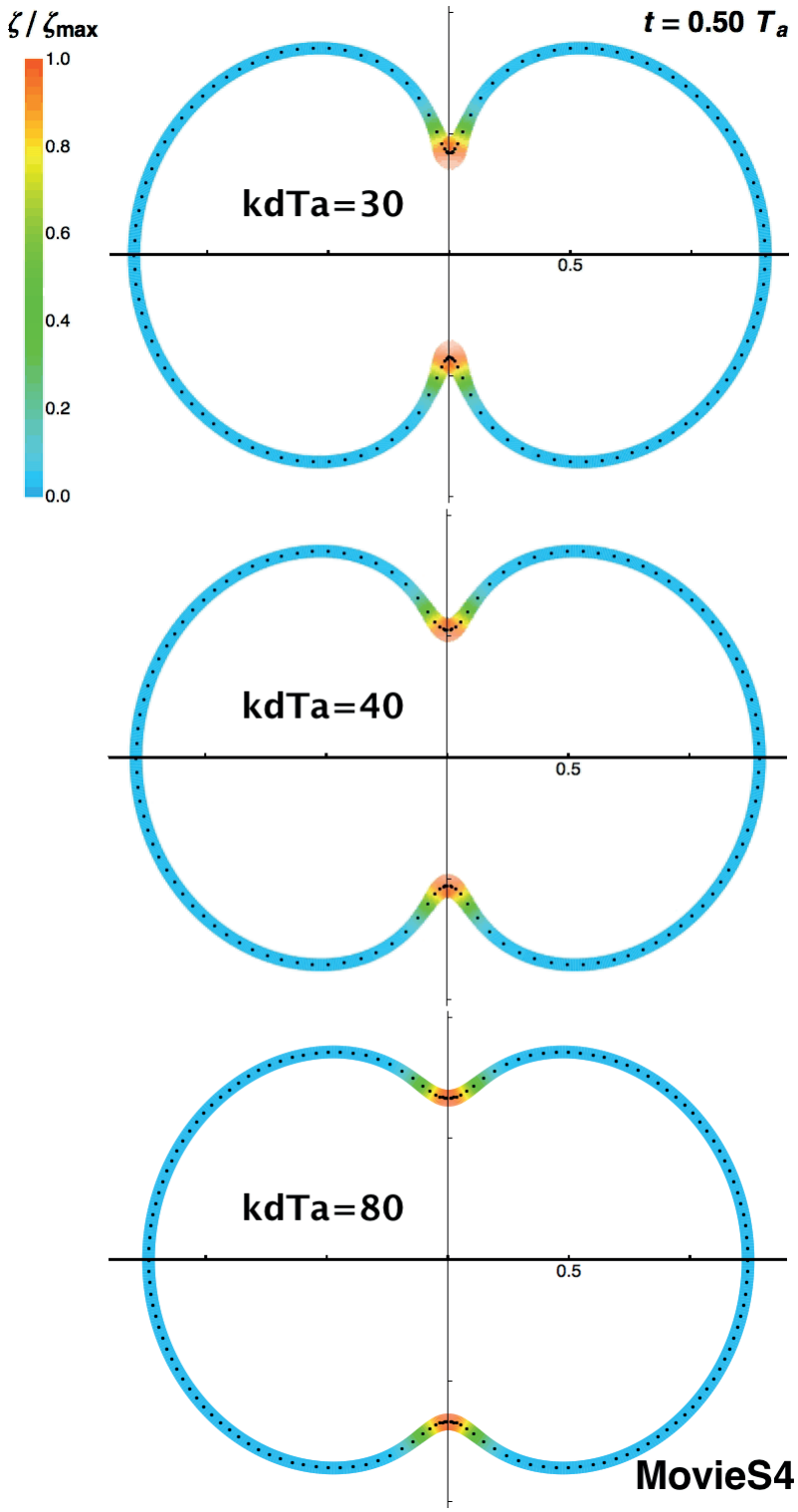

MOVIE S4: Comparison of the cell shape and cortex thickness dynamics in a section plane $(\mathbf{e}_z, \mathbf{e}_r)$ for the three turnover rates $k_d\,T_a = 30$, $k_d\,T_a = 40$ and $k_d\,T_a = 80$ at fixed equatorial activity amplitude $\delta\zeta^\infty = 75$, corresponding respectively to the furrow radius time evolutions ①, ② and ③ in Fig. 4 (Main text). A few Lagrangian points are represented within the membrane to capture the cortical flows

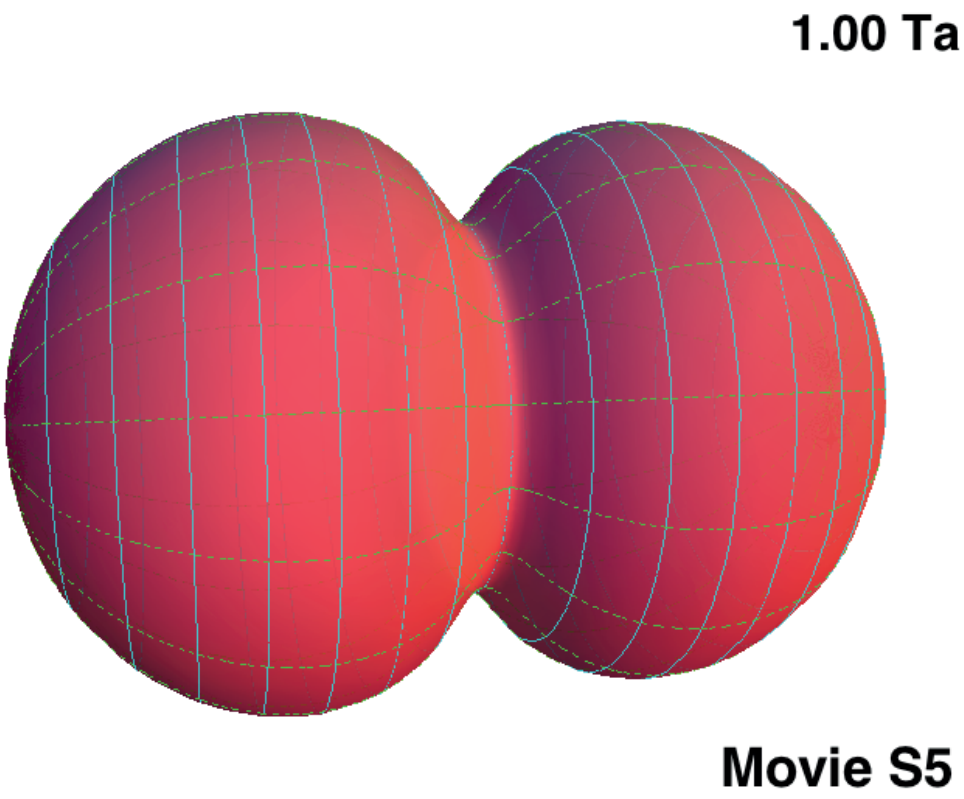

MOVIE S5: Dynamics of the cell shape in 3 dimensions, corresponding to Fig. 1 (Main text) and Movie S1.